ELSEVIER

Energy and Buildings 26 (1997) 317–325

ENERGY AND BUILDINGS

Simulation study on an air flow window system with an integrated roll screen

Jun Tanimoto [a], Ken-ichi Kimura [b]

[a] *School of Engineering Sciences, Kyushu University, Kasuga-shi, Fukuoka, 816 Japan*
[b] *Department of Architecture, School of Science and Engineering, Waseda University, Tokyo, Japan*

Received 26 April 1996; accepted 11 February 1997

Abstract

A numerical calculation procedure for an air flow window (AFW) system integrated with a roll screen is presented. Both heat and air flows within the window elements such as the outside pane of glass, the outside air space, a venetian blind, the inside air space and a roll screen, are taken into account by considering the thermal and air flow networks. Agreements between measured and calculated results of temperatures and pressure differences through a series of experiments carried out in an environmental test chamber were observed. To identify the quantitative characteristics of an AFW integrated with a roll screen, a series of numerical simulations were performed with the results from using a large resistance to the air flow from the upper half area of the roll screen. These show that this was effective in terms of thermal characteristics and suggest that a tightly-meshed roll screen, situtated in the upper half area, is suitable for both environmental and design reasons. If the heated air flow generated from the inside air space to the room were dispersed properly, the thermal efficiency of the AFW integrated with a roll screen would be equal to a conventional AFW system. The effect of a cold draft passing though the roll screen is also discussed. © 1997 Elsevier Science S.A.

Keywords: Simulation study; Air flow window system; Integrated roll screen; Numerical calculation; Thermal characteristics; Japan

1. Introduction

In order to reduce the air conditioning load in a perimeter zone of office buildings, the so-called perimeterless techniques, such as AFW and double skin construction, are regarded as effective solutions. Several early works on the perimeterless method have been proposed in Europe and America [1]. In particular, the AFW system was employed in Scandinavian countries in the mid-80s [2–4]. In the United States, the first AFW was installed in 1980 in an office building in Portland, Oregon [5]. Since then, a number of studies on buildings with an AFW have been completed, showing that they are highly energy efficient.[6–8]. In contrast, Japanese office buildings with single-glazed windows and a venetian blind are still common owing to the high cost of glass in Japan compared with other countries. Recently, a simple construction of an AFW system has been proposed [9] in which a roll screen was used instead of the inside pane of a glass window. In this system, undesirable hot air will flow from the air space to the room during the summer and a cold draft will be produced in the winter due to the air flow though the roll screen. This has made it necessary to quantify simultaneous heat and air flows within the window system, which have not been taken into account in the calculation procedures for a conventional window system. This paper deals with a calculation procedure based on the simultaneous thermal and air flow network. The results are confirmed experimentally.

PII S0378-7788(97)00012-1

2. Calculation model

2.1. Calculation procedure

The AFW system used for the calculation is shown schematically in Fig. 1. By considering heat conduction, convection, absorption of solar radiation and long wave radiation and heat transfer derived from air flows, heat balances at every discrete node can be obtained as shown in Eqs. (1)–(7) in the Appendix. These equations can be converted into a vector–matrix, see Eq. (8), by using the thermal network method [10]. If the problem needs to be solved for a whole room thermal system rather than just a window system, a set of heat balance equations for other discrete nodes such as the floor, ceiling and walls have to be incorporated into Eq. (8) for a simultaneous solution.

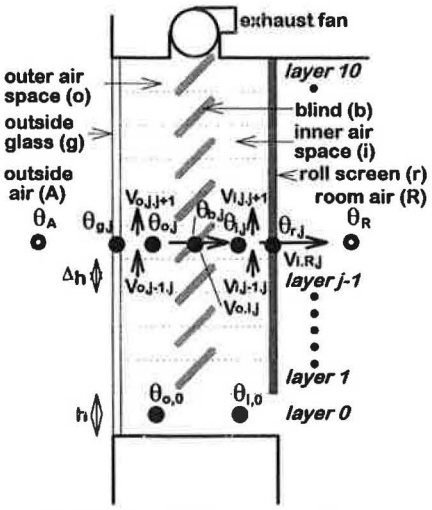

Fig. 1. Object AFW system for calculation.

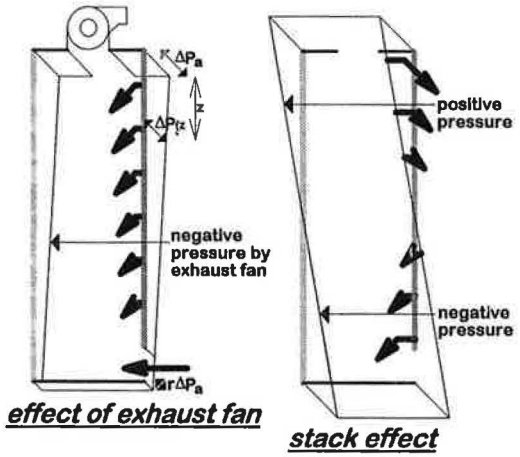

Fig. 2. Two influences on the air flow.

In contrast, the influence of air flow on heat balance can be divided into two effects (i) the negative pressure by an exhaust fan and (ii) the pressure distribution by a stack effect within the air space as shown schematically in Fig. 2. The pressure difference between the outside air space and the inside air space and the one between the inside air space and the room are expressed in Eqs. (9) and (10), respectively. By the air flow network method, Eqs. (11)–(13) can be combined to yield Eq. (14) which expresses air volume balance within the air space. In Eq. (13), based on the results of the previous experiment [11], the air flow rate through the roll screen was assumed to be regulated by a linear function of the pressure difference. Air flow rate from the outside air space to the inside air space through the venetian blind can be calculated by Eq. (15).

A numerical solution was made using an implicit type of finite difference method in which a small time step was selected because of non-linearity of these equations. In solving non-linear equations that consider heat transfer and air flow simultaneously, an iterative process between Eq. (8) and Eq. (14) was applied.

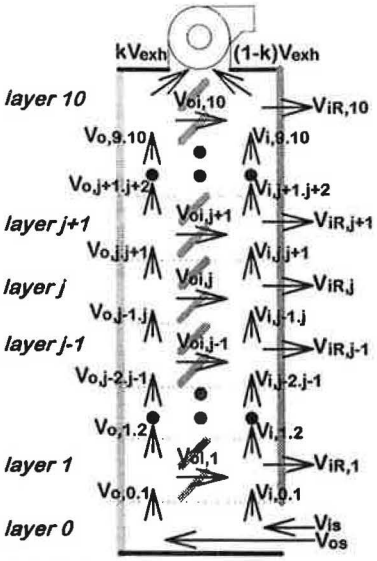

Fig. 3. Symbols for Appendix and Nomenclature across the AFW.

Fig. 3 shows the symbols used in the Appendix and Nomenclature.

2.2. *Validation for the calculation procedure*

Fig. 4 compares the calculated and measured pressure differences across the roll screen and the air velocities at the end slit of the roll screen for air exhaust rates of 0, 60 and 100 $m^3/h/m$. The exhaust air rate in $m^3/h/m$ indicates the rate of air flow per an unit length of window depth. The experimental validation was carried out in an environmental test chamber in which indoor temperature (26°C), relative humidity (50%), outdoor temperature (34°C) and incident radiation on a vertical surface by an artificial solar simulator (700 W/m^2), were precisely controlled.

With the increase in the exhaust air flow rate, a larger discrepancy between the calculated and measured pressure difference was observed. However, the pattern of pressure difference distributions can be considered quite similar to each other.

Fig. 5 shows the relationship between the calculated and measured temperatures at all measuring points. Although a few calculated values were found to be considerably different from the measured ones for 0 and 60 $m^3/h/m$, a high correlation could be obtained. The calculated temperature distribution for 60 $m^3/h/m$ is shown in Fig. 6 together with the measured values. As can be observed, discrepancies in temperature of the inside air space and the roll screen are significant at the highest measuring point. Three-dimensional complicated air flow within the air space is considered to give rise to those discrepancies and this was not taken into account in the present calculation procedure. There are also several possibilities such as uncertainty of the convective heat transfer coefficient on the roll screen surface, short circuit air flow around the top of the inside air space caused by the exhaust fan, and inevitable experimental errors. However, it would

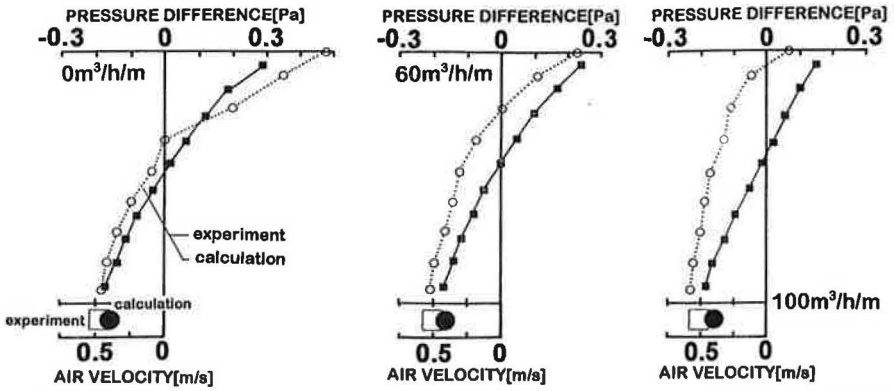

Fig. 4. Comparison between calculated and measured pressure differences and air velocities for three different rates of air flow. Closed squares are the calculated static pressure differences against the room air. Open circles are the measured static pressure differences at the calculated points.

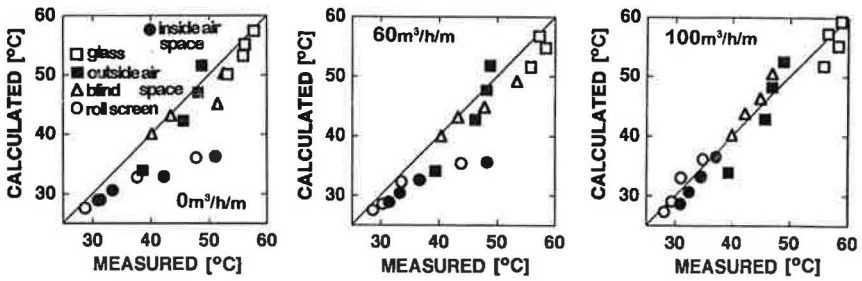

Fig. 5. Comparison between calculated and measured temperatures for three different rates of air flow. Measured temperatures are interpolated at the heights of calculated points.

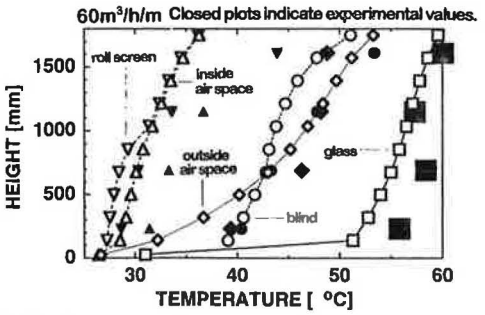

Fig. 6. Calculated vs. measured temperature distribution for a rate of air flow of 60 $m^3/h/m$. Closed symbols are the measured temperatures acquired at four heights.

be impossible to explain completely those discrepancies, even if a detailed CFD calculation procedure were to be applied.

Therefore, based on the previously-mentioned comparison, it is considered possible to simulate a distribution of pressure difference and temperature using the proposed method within a certain accuracy.

3. Numerical experiment

3.1. Simulation parameters and conditions

To identify the influence of design factors, such as air flow resistance of the roll screen and exhaust air rate, on the thermal characteristics of the AFW system integrated with a roll screen quantitatively, a series of simulations was performed using the proposed calculation method. In particular, emphasis has been placed on the near-window thermal comfort in the office building in order to assess quantitatively the undesirable effects of hot summer air and cold winter drafts through the air-permeable roll screen, and their prevention. In the simulation study, the air flow resistance of the roll

Table 1
Factors and levels of numerical experiment

Factors	Levels
A. Air flow resistance (Pa s/m)	5 (case A.1); 10 (standard case); 20 (case A2); upper half area 20 (case A3); lower half area 10
B. Exhaust air rate ($m^3/h/m$)	0 (case B1); 20 (case B2); 40 (standard case); 80 (case B3)
C. Height of window (m)	1.4 (case C1); 2.0 (standard case); 5.0 (case C2)

Air flow resistance of the standard case, ($a = 10$ Pa s/m), is equal to the value of the roll screen used in the experiment for validation.
For summer conditions, conventional type AFWs were investigated for factors B and C for comparison. The results of calculated heat fluxes for the window systems are shown schematically in Fig. 8.

Table 2
Miscellaneous assumptions for calculation

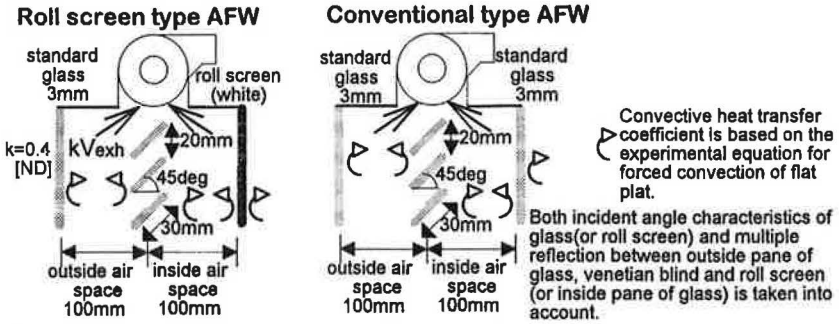

for summer calculation
room air temperature = 26°C; outdoor air temperature = 33°C; outdoor air humidity ratio = 20 g/kg; normal direct solar radiation = 872 W/m²; horizontal sky solar radiation = 145 W/m², cloud amount = 0; facade = west; location = Tokyo; time = 16 h.

for winter calculation
indoor air temperature = 22°C; outdoor air temperature = 0°C; outdoor air humidity ratio = 1.5 g/kg; solar radiation = 0 W/m²; cloud amount = 0.

screen, the exhaust air flow rate and the window height were picked up as three main factors, as shown in Table 1. To evaluate the rate of heated air flow through the roll screen into the room caused by a stack effect in summer and a cold draft in winter, peak outdoor conditions were assumed for summer and winter. For summer conditions, calculations using the conventional type AFW system were carried out for comparison. Other assumptions for calculation are summarized in Table 2. Calculations were performed under unsteady-state conditions, but solutions were obtained during a daily periodic steady state.

3.2. Results and discussion of summer cases

Simulation results of temperature distribution and rate of air flow of the standard case are shown in Fig. 7 together with

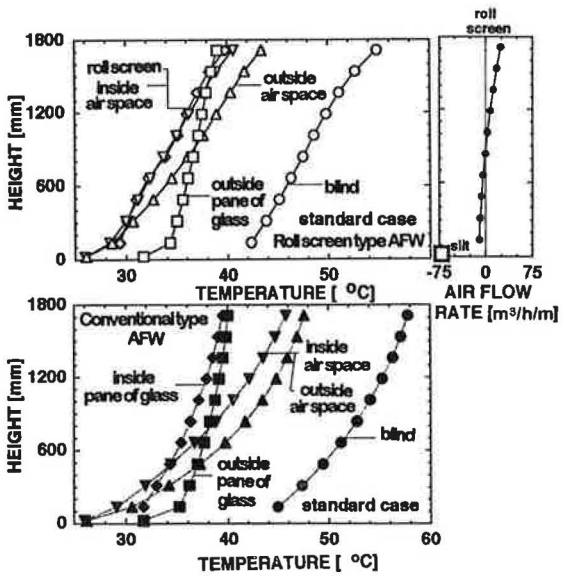

Fig. 7. Simulation results of the standard case for summer conditions.

the results of a conventional type AFW. It is well recognized that the air, whose temperature is around 38°C, is transported from the inside air space to the room through the upper part of the roll screen. As can be observed, the temperatures of a venetian blind, outside air space and inside air space in the case of roll screen type, is lower than in the case of conventional type. This is due to the fact that, in the conventional type AFW, the heated air within the air space is effectively exhausted by the fan due to the airtightness of the inside pane of glass.

Simulation results of heat fluxes related to the heat balance at the window system are shown in Fig. 8. The upper part of Fig. 8 shows the results of roll screen type AFW cases; the lower one indicates the conventional type AFW results. Every heat flux has value per an unit length of window depth. The resistance of the air flow increases, the hot air exhausted increases and the transported air decreases. This is because the roll screen with a large air flow resistance is efficient in keeping the heated air in the air space. Observing these results, it can be seen that the exhausted and transported heat of case A3 are almost equivalent to those of case A2. This tendency suggests the upper half area of the tight meshed roll screen is more efficient from the point of thermal characteristics. In contrast, for the lower half, it is applicable to use a loose-meshed roll screen. This has the further advantage that it allows a comfortable view line.

The effect of the rate of exhaust air can be clearly seen; the greater the rate, the more heat is exhausted and the heat transmitted decreases. However, it is thought that this relationship gradually levels out.

Observing the effect of the height of the window, less heat was exhausted and more heat transported for C2 compared with results of from the other levels. This is because a large window height increases significantly the stack effect. It is important, therefore, to be careful in applying the roll screen

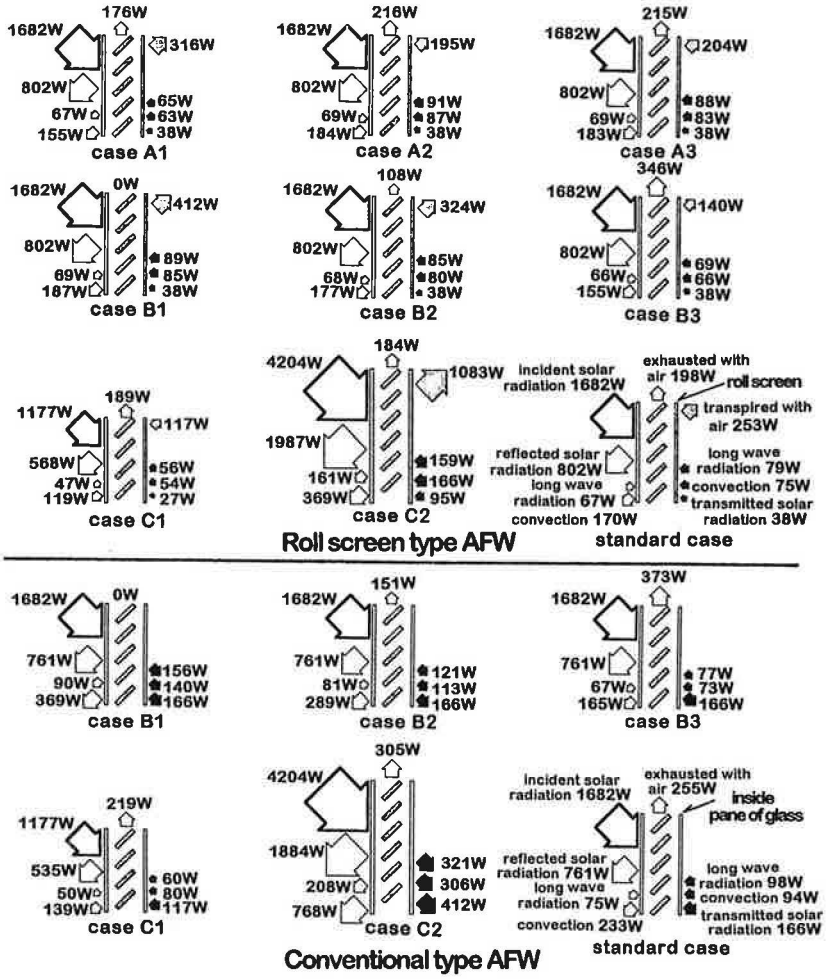

Fig. 8. Simulation results of heat fluxes related to the heat balance at the window system.

type AFW system to high areas such as stairwells and hallways.

Comparing the results of the roll screen type with those of the conventional type AFW, a greater rate of heat exhaustion by the fan is found in the conventional type owing to the airtightness of the inside pane of glass which prevents heated air from flowing into the room as opposed to the air penetration of the roll screen. However, if the transmitted heat flow from the inside air space to the room through the upper area of the roll screen could be dispersed properly by some mechanical technique such as air inlets in the ceiling of the perimeter zone, it would be possible for the thermal efficiency of the roll screen type to be equivalent to that of the conventional type AFW.

3.3. Results and discussion of winter cases

Simulation results of temperature distribution of the inside air space, temperature of the outside air space at layer 0 and rate of air flow through the roll screen are shown in Fig. 9. HLCD is heat loss brought about by the cold draft, defined as

$$HLDC(W) = -C_{Pa}\gamma(\theta_{O,0})V_{os}(\theta_R - \theta_{O,0}) - C_{Pa}\gamma(\theta_{i,0})V_{is}(\theta_R - \theta_{i,0}) - C_{Pa}\sum_{j=1}^{10}\gamma(\theta_{i,j})V_{i.R,j}(\theta_R - \theta_{i,j})$$

In this equation, the first term on the right-hand side should be calculated only if $\theta_R > \theta_{o,0}$ and $V_{os} < 0$. In addition, the second and third terms on the right-hand side need to be calculated only if $\theta_R > \theta_{i,0}$ and $V_{is} > 0$, $\theta_R > \theta_{i,j}$ and $V_{iR,j} < 0$.

As can be observed, a larger air flow resistance or a greater exhaust air rate can reduce the hazards of cold draft. However, the parameters assumed, as shown in Table 1, are not sufficient to eliminate the cold draft completely. It is confirmed that a high window is also disadvantageous. In an office building, the cold winter draft from the window is one of the most serious problems, leading to thermal discomfort for those placed near to it.

Fig. 10 shows the results of additional simulations performed for two cases, (i) with the end slit of the roll screen closed, that is, the roll screen was shut down entirely (case RSD), and (ii) with the roll screen entirely shut down and an assumed exhaust air rate of 130 $m^3/h/m$. Other conditions

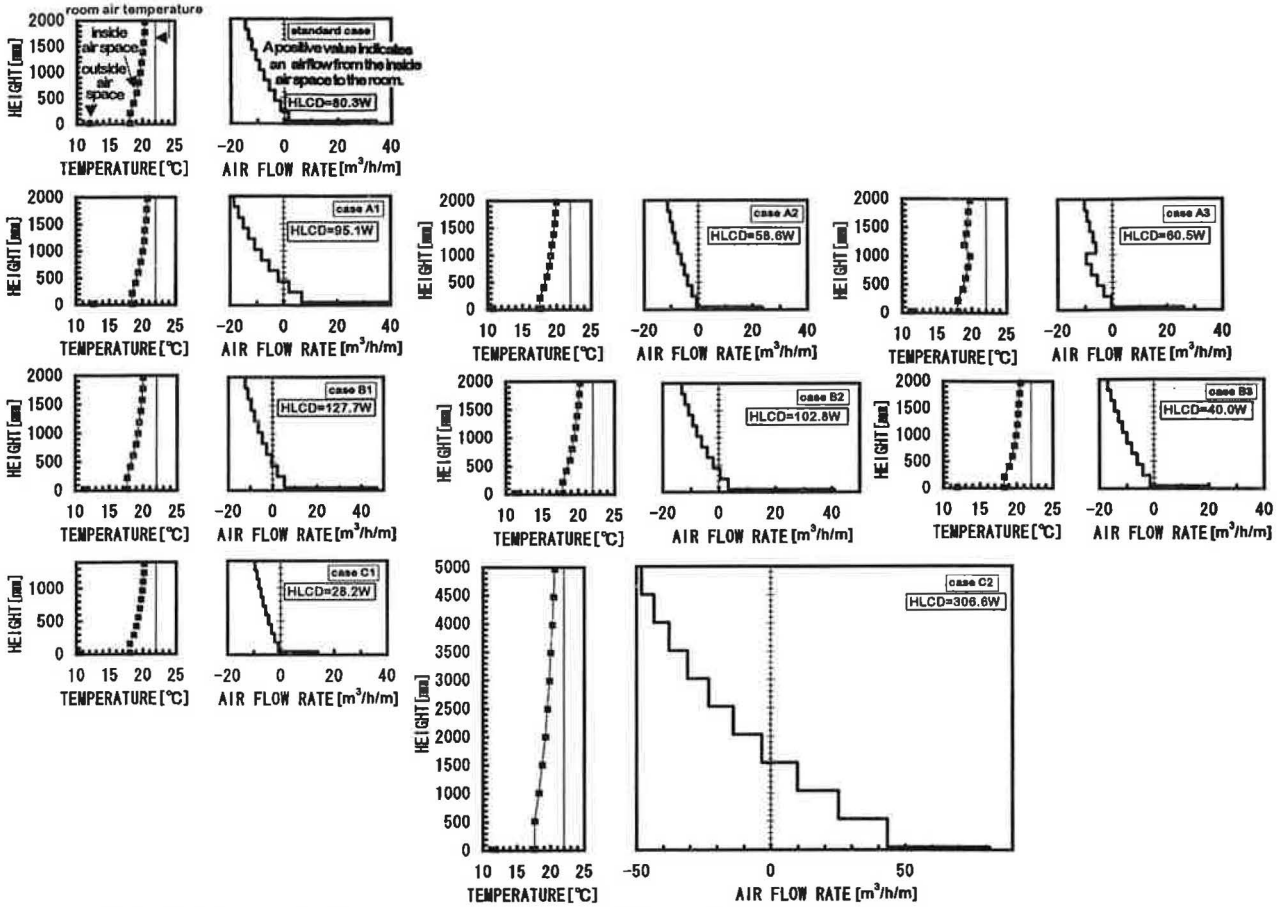

Fig. 9. Simulation results of temperatures of the air space and the rate of air flow transmitted through the roll screen and HLCD.

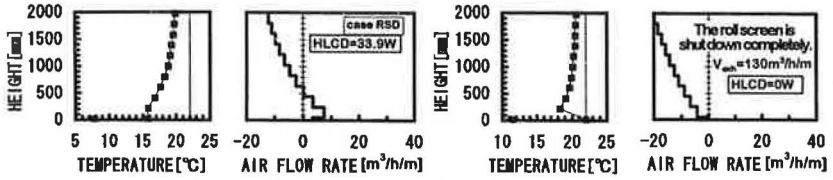

Fig. 10. Additional simulation results for reference.

for calculation except for these were assumed to be the same as for the standard case. Results indicate that to close the end slit of the roll screen by shutting down is effective in restricting the cold draft to a some degree. However, by closing the end slit of the roll screen and increasing the exhaust air rate to 130 $m^3/h/m$, the cold draft can be avoided completely.

4. Conclusions

The following conclusions can be drawn from this study.

(i) To evaluate thermal characteristics of AFW constructed with roll screen quantitatively, a calculation procedure based on both thermal and air flow network method was developed and proposed.

(ii) The proposed calculation method has been validated by comparing the pressure differences and temperatures between those measured and the ones calculated.

(iii) The results of simulation for a summer season suggest that a large air flow resistance of the upper half area of the roll screen would be effective in preventing the heated air within the air space from flowing out into the room, which is preferable for design reasons as well.

(iv) If the heated air moving from the inside air space to the room was dispersed properly, thermal efficiency of the roll screen type AFW would be equal to conventional type AFW system.

(v) The results of the simulation for the winter season indicated that it was impossible to avoid completely the cold draft transmitted through the lower area of roll screen during normal operating conditions. However, closing the end slit of the roll screen is effective in restricting the cold draft.

(vi) Owing to the thermal characteristics of the roll screen type AFW, it is recommended not to apply this type of screen in such area as entrance halls and stairwells.

Taking into consideration all these points, the AFW integrated with a roll screen is a acceptable window system for use by architects and engineers.

5. Nomenclature

a	air flow resistance of the roll screen (Pa s/m)
A	area (m^2)
a_D	overall absorptance for direct solar radiation (–)
a_S	overall absorptance for diffused solar radiation (–)
C_{Pg}	specific heat of glass (J/kg K)
g	acceleration of gravity (m/s^2)
h	height of end slit (m)
I_D	incident direct solar radiation (W/m^2)
I_S	incident diffuse solar radiation (W/m^2)
k	ratio of exhaust air rate from outside air space to total exhaust air rate (–)
$K_{go,j}$	overall heat conductance between outside pane of glass and outside air space considering air velocity within outside air space at layer j (W/m^2K)
$\mathbf{K}$	heat conductance matrix
$\boldsymbol{K}_o\{\boldsymbol{\theta}_o\}$	vector–matrix product for boundary condition by convective heat transfer
$\mathbf{M}$	heat capacitance matrix
R	net long wave radiation rate (W/m^2)
$\boldsymbol{R}_{AD}\{r_{ad}\}$	vector–matrix product for boundary condition by radiation
Δh	discrete height of roll screen (m)
ΔP	pressure difference
$\Delta P(z)$	negative pressure by exhaust fan (Pa) ($=-\Delta Pa^*(1-r)^*z/(10\Delta h+h)+\Delta Pa$)
ΔP_a	negative pressure at air inlet of exhaust fan (Pa)
r	defined parameter ($0 \le r \le 1$) (–)
t	time (h)
T_m	mean temperature of opposite surfaces (K)
V_{exh}	exhaust air rate (m^3/h)
$V_{o,j-1,j}$	air flow rate from layer $j-1$ to layer j at outside air space (m^3/h)
z	distance from air inlet of exhaust fan to the point (m)

Greek letters

α	flow coefficient (–)
ϵ	emittance (–)
γ	specific weight (kg/m^3)
$\gamma(\theta)$	specific weight of air at θ°C (kg/m^3)
θ	temperature (°C)
$4\epsilon\sigma T_m^3$	linearized radiative heat transfer coefficient (W/m^2K)
σ	Stefan–Boltzmann constant (W/m^2K^4)
$\alpha_{os}A_{os}$	effective slit opening area from room to outside air space via end slit of roll screen, inside air space and end slit of venetian blind (m^2) ($=\{1/(0.5\alpha_{rs}A_{rs})^2+1/(\alpha_{bs}A_{bs})^2\}^{-0.5}$)
$\{\boldsymbol{\theta}\}$	vector of unknown temperature

Subscripts

a	air
Ag, j	between outdoor air and inside pane of glass
b	slit of venetian blind
bs	end slit of venetian blind
b, j	layer j element of venetian blind
bi, j	between venetian blind and inside air space
g	glass
i, $j-1.j$	from layer $j-1$ to layer j at inside air space
ir, j	between inside air space and room air
iR, j	from inside air space to room at layer j
is	from room to inside air space through end slit of roll screen
ob, j	between outside air space and venetian blind
oi, j	from outside to inside air space at layer j
os	from room to outside air space through end slit of roll screen
r	roll screen
rs	end slit of roll screen
r, j	layer j of roll screen

Acknowledgements

The authors wish to acknowledge Mr Hirayama, Mr Yamaguchi and Miss Hisamoto of Obayashi Co., and Dr Koganei and Mr Lin of the Research and Development Center of Asahi Kogyosha Co. for the provision of a series of experimental data. We are grateful to Dr Hayashi of Kyushu University for his kind advice and assistance in data processing.

Appendix A

Based on the thermal network method, heat balances at every discrete node are expressed as following set of equations.

A.1. at the outside pane of glass

$$C_{Pg}\gamma_g\frac{d\theta_{g,j}}{dt}=K_{Ag}(\theta_A-\theta_{g,j})+K_{go,j}(\theta_{o,j}-\theta_{g,j})+4\epsilon\sigma T_m^3(\theta_{b,j}-\theta_{g,j})+a_{D,g}I_D+a_{S,g}I_S-R_g \quad (1)$$

A.2. at the outside air space

A.2.1. for layers 1–10

$$\Delta hC_{Pa}\gamma_a\frac{d\theta_{o,j}}{dt}=\Delta hK_{go,j}(\theta_{g,j}-\theta_{o,j})+\Delta hK_{ob,j}(\theta_{b,j}-\theta_{o,j})+C_{Pa}\gamma(\theta_{o,j-1})V_{o,j-1,j}(\theta_{o,j-1}-\theta_{o,j})-C_{Pa}\gamma(\theta_{i,j})V_{o,i,j}(\theta_{i,j}-\theta_{o,j}) \quad (2)$$

If $V_{o,j-1,j}<0$, the third term on the right-hand side can be neglected. If $V_{o,i,j}\geq 0$, the fourth term on the right-hand side can be neglected.

A.2.2. for layer 0

$$hC_{Pa}\gamma_a\frac{d\theta_{o,0}}{dt}=hK_{go,0}(\theta_{g,0}-\theta_{o,0})+C_{Pa}\gamma(\theta_R)V_{os}(\theta_R-\theta_{o,0})-C_{Pa}\gamma(\theta_{o,1})V_{o,0,1}(\theta_{o,1}-\theta_{o,0}) \quad (3)$$

If $V_{os}<0$, the second term on the right-hand side can be neglected. If $V_{o,0,1}\geq 0$, the third term on the right-hand side can be neglected.

A.3. at the venetian blind

$$0=K_{ob,j}(\theta_{o,j}-\theta_{b,j})+K_{bi,j}(\theta_{i,j}-\theta_{b,j})+4\epsilon\sigma T_m^3(\theta_{g,j}-\theta_{b,j})+4\epsilon\sigma T_m^3(\theta_{r,j}-\theta_{b,j})+a_{D,b}I_D+a_{S,b}I_S \quad (4)$$

A.4. at the inside air space

A.4.1. for layers 1–10

$$\Delta hC_{Pa}\gamma_a\frac{d\theta_{i,j}}{dt}=\Delta hK_{bi,j}(\theta_{b,j}-\theta_{i,j})+\Delta hK_{ir,j}(\theta_{r,j}-\theta_{i,j})+C_{Pa}\gamma(\theta_{i,j-1})V_{i,j-1,j}(\theta_{i,j-1}-\theta_{i,j})+C_{Pa}\gamma(\theta_{o,j})V_{o,i,j}(\theta_{o,j}-\theta_{i,j})-0.5[C_{Pa}\gamma(\theta_R)V_{i,R,j}(\theta_R-\theta_{i,j})]-0.5[C_{Pa}\gamma(\theta_{r,j})V_{i,R,j}(\theta_{r,j}-\theta_{i,j})] \quad (5)$$

If $V_{i,j-1,j}<0$, the third term on the right-hand side can be neglected. If $V_{o,i,j}<0$, the fourth term on the right-hand side can be neglected. If $V_{i,R,j}\geq 0$, the fifth term on the right-hand side can be neglected.

A.4.2. for layer 0

$$hC_{Pa}\gamma_a\frac{d\theta_{i,0}}{dt}=C_{Pa}\gamma(\theta_R)V_{is}(\theta_R-\theta_{i,0})-C_{Pa}\gamma(\theta_{i,1})V_{i,0,1}(\theta_{i,1}-\theta_{i,0}) \quad (6)$$

If $V_{is}<0$, the first term on the right-hand side can be neglected. If $V_{i,0,1}\geq 0$, the second term on the right-hand side can be neglected.

A.5. at the roll screen

$$C_{Pr}\gamma_r\frac{d\theta_{r,j}}{dt}=K_{ir,j}(\theta_{i,j}-\theta_{r,j})+K_{rR,j}(\theta_R-\theta_{r,j})+4\epsilon\sigma T_m^3(\theta_{b,j}-\theta_{r,j})-0.5C_{Pa}\gamma(\theta_R)\times V_{i,R,j}(\theta_R-\theta_{r,j})+a_{D,r}I_D+a_{S,r}I_s-R_r \quad (7)$$

If $V_{i,R,j}\geq 0$, the fourth term on the right-hand side can be neglected.

$$\{\boldsymbol{\theta}\}_{k+1}=\mathbf{A}^{-1}\cdot\{\mathbf{B}\cdot\{\boldsymbol{\theta}\}_{k+1}+\mathbf{K}_0\cdot\{\boldsymbol{\theta}_o\}+\mathbf{R}_{AD}\cdot\{r_{ad}\}\} \quad (8)$$

where $\mathbf{A}=(\mathbf{M}/\Delta t-p\cdot\mathbf{K})$; $\mathbf{B}=(\mathbf{M}/\Delta t+(1-p)\cdot\mathbf{K}]$.

For calculating the air flow, the air flow network method is applied. The pressure difference is calculated from the difference in the specific weights of the air in the outside and inside air spaces at layer j can be written as:

$$\Delta P_{oi,j}=gh[\gamma(\theta_{i,0})-\gamma(\theta_{o,0})]+g\sum_{n=1}^{j}\Delta h[\gamma(\theta_{i,n})-\gamma(\theta_{o,n})] \quad (9)$$

The pressure difference between the inside air space and the room at layer j, expressed in Eq. (10), is affected by the difference in the specific weight of the air and the negative pressure caused by the exhaust fan.

$$\Delta P_{iR,j}=-\Delta P(z)+gh[\gamma(\theta_R)-\gamma(\theta_{i,0})]+g\sum_{n=1}^{j}\Delta h[\gamma(\theta_R)-\gamma(\theta_{i,n})] \quad (10)$$

The rates of air flow from the room to the outside air space and to the inside air space though a end slit of the roll screen are expressed in Eqs. (11) and (12), respectively.

$$V_{os}=3600\alpha_{os}A_{os}\left(2\frac{g}{\gamma}\right)^{0.5}\times\left\{\frac{\Delta P(z)}{g}+0.5h[\gamma(\theta_{o,0})-\gamma(\theta_{i,0})]\right\}^{0.5} \quad (11)$$

If $(\Delta P(z)/g+0.5h\{\gamma(\theta_{o,0})-\gamma(\theta_R)\})\geq 0$, $\gamma=\gamma(\theta_R)$. If $(\Delta P(z)/g+0.5h\{\gamma(\theta_{o,0})-\gamma(\theta_R)\})<0$, $\gamma=\gamma(\theta_{o,0})$.

$$V_{is}=3600\alpha_{rs}0.5A_{rs}\left(\frac{2g}{\gamma}\right)^{0.5}\times\left\{\Delta\frac{P(z)}{g}+0.5h[\gamma(\theta_{i,0})-\bar{\gamma}(\theta_R)]\right\}^{0.5} \quad (12)$$

If $(\Delta P(z)/g+0.5h\{\gamma(\theta_{i,0})-\gamma(\theta_R)\})\geq 0$, $\gamma=\gamma(\theta_R)$. If $(\Delta P(z)/g+0.5h\{\gamma(\theta_{i,0})-\gamma(\theta_R)\})<0$, $\gamma=\gamma(\theta_{i,0})$.

The rate of air coming from the inside air space to the room at layer j is written in Eq. (13).

$$V_{iR} = \sum_{j=1}^{10} \Delta P_{iR,j}(3600 A_{b,j}/a) \quad (13)$$

$$V_{os} + V_{is} - V_{iR} - V_{exh} = 0 \quad (14)$$

Eq. (14) describes the air flow balance within the whole air space, which is numerically solved with Eq. (8) simultaneously.

$$V_{oi,j} = \frac{(V_{os} - kV_{exh})}{\left[3600\alpha_b A_{b,j} \sum_{j=1}^{10} \left(\frac{2}{\gamma}\right)^{0.5} \Delta P_{oi,j}^{0.5}\right]} \left[3600\alpha_b A_{b,j} \left(\frac{2}{\gamma}\Delta P_{oi,j}\right)^{0.5}\right] \quad (15)$$

If $\Delta P_{oi,j} \geq 0$, $\gamma = \gamma(\theta_{o,j})$. If $\Delta P_{oi,j} < 0$, $\gamma = \gamma(\theta_{i,j})$. These simultaneous equations include fifty − four unknowns, fifty-three temperatures and $\Delta P(z)$, with assumed parameters r and k.

References

[1] A.Punttila and S.Enbom, Heat transfer calculations of different types of window systems, *4th Int. Symp. on the Use of Computers for Environmental Engineering Related to Buildings, Tokyo, Japan*, 1983.

[2] Performance of extract air windows, *Final Rep.*, Technical Research Center of Finland, Helsinki, Finland, 1977.

[3] M. Gefwert and O. Sodergen, Annual energy loss though a ventilation window, *Document D1*, Swedish Council for Building Research, Stockholm, Sweden, 1981.

[4] S. Enbom, *Solar Energy Recovery with Extract Air Window System*, Helsinki University of Technology, Helsinki, Finland, 1977.

[5] H. Ripatti, Airflow window system-making fenestration the solution rather than the problem, *ASHRAE Trans., 84-18* (1984) 18.

[6] Evaluation of air flow windows, *Final Rep.*, Lawrence Berkeley Laboratory, Berkeley, CA, 1981.

[7] D. Aitken, The use of air flow windows and blinds for building thermal control and for solar-assisted heating, cooling and Lighting, *6th Int. Passive Solar Conference*, American Section of International Solar Energy Society, Portland, OR, 1981.

[8] J. Gabirelsson, Extract air window; a key to better heat economy in buildings, *10th World Energy Conference, Istanbul, Turkey*, 1977.

[9] M. Hirayama, K. Yamaguchi and H. Kaneda3, Experimental study on the air flow window constructed with roll shade Part 1, *Proc. Ann. Meeting, SHASEJ*, Vol. 2 1993 (in Japanese).

[10] J. Tanimoto and K. Kimura, Fundamental study on the indoor humidity regulation characteristics of porous building materials, *Proc. Int. CIB W67 Symp. on Energy, Moisture and Climate in Buildings, Rotterdam, ND*, 1990.

[11] M. Hirayama, K. Yamaguchi and H. Kaneda, Experimental study on the air flow window constructed with roll shade Part 2, *Proc. Ann. Meeting, SHASE*, 1994 (in Japanese).